Longshore sediment transport by large-scale lake circulations at low-energy, non-tidal beaches

A field and model study

Ton, Anne M.; Vuik, Vincent; Aarninkhof, Stefan G.J.

DOI
10.1016/j.coastaleng.2022.104268

Publication date
2023

Document Version
Final published version

Published in
Coastal Engineering

Citation (APA)
Ton, A. M., Vuik, V., & Aarninkhof, S. G. J. (2023). Longshore sediment transport by large-scale lake circulations at low-energy, non-tidal beaches: A field and model study. *Coastal Engineering*, *180*, Article 104268. https://doi.org/10.1016/j.coastaleng.2022.104268

Coastal Engineering 180 (2023) 104268

Contents lists available at ScienceDirect

Coastal Engineering

journal homepage: www.elsevier.com/locate/coastaleng

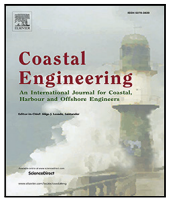

Longshore sediment transport by large-scale lake circulations at low-energy, non-tidal beaches: A field and model study

Anne M. Ton [a,*], Vincent Vuik [a,b], Stefan G.J. Aarninkhof [a]

[a] Civil Engineering and Geosciences, Delft University of Technology, P.O. Box 5048, Delft, 2600 GA, The Netherlands
[b] HKV Consultants, P.O. Box 2120, Lelystad, 8203 AC, The Netherlands

ARTICLE INFO

Dataset link: https://waterinfo-extra.rws.nl/projecten/@205186/houtribdijk/

Keywords:
Low-energy
Sandy lake beach
Morphodynamics
Large-scale lake circulation
Longshore transport
Delft3D

ABSTRACT

Low-energy, non-tidal lake beaches are known to be subject to longshore morphodynamics, but little is known about how they are driven by wind and wave-driven currents. Lake Markermeer is a shallow (~4 m deep), wind-dominated lake, of approximately 700 km^2. A gradient in wind-induced water level set-up at the leeward shore induces a flow from the shallower to the deeper parts of the lake, thereby generating a large-scale, horizontal circulation. Flow measurements and results from a numerical Delft3D model of the lake show that these circulations impact the nearshore currents greatly, even more than wave-driven longshore currents for most wind conditions. From nearshore measurements at the first study site in lake Markermeer, we found a clear relation between longshore sediment transport capacity and the measured longshore volume flux. The model numerical can predict flow direction and magnitude for any wind condition. Using wind statistics, the net transport capacity for a short period or a long term mean can be predicted. The relation is confirmed for a second study site, which shows a distinct net transport capacity that could not be explained from wave-driven longshore flow alone. Concluding, large-scale lake circulations are of great significance for the morphological development of low-energy, non-tidal beaches in shallow, wind-driven water bodies. Knowledge of these circulations and their dependence on wind characteristics is a crucial factor to better understand and predict sediment losses of lake beaches.

1. Introduction

Hydrodynamic and morphological processes at low-energy or sheltered beaches can be significantly different compared to open, high-energy coasts, contrary to what was thought in the past (Lorang et al., 1993; Eliot et al., 2006; Nordstrom and Jackson, 2012; Vila-Concejo et al., 2020). Low-energy beaches, commonly characterized by a small prevailing wave height and limited storm wave height, are in all definitions considered to have storm-driven morphodynamics.

Ton et al. (2021) have set up a conceptual model for morphological development of low-energy, sandy coasts during calm and storm conditions in the cross-shore direction, based on data from newly-constructed lake beaches. However, longshore morphological development is also deemed important. When low-energy environments are (partially) sheltered, large alongshore variations in wave energy can be found. Moreover, if waves are fetch-limited and therefore have a short period, they are less affected by refraction and increase the potential for strong wave-driven longshore currents. Dominance of cross-shore or longshore processes is dependent on shoreline orientation to the dominant winds and fetch, and the presence of (shore-normal) obstacles, such as groynes, that act as sediment traps (Jackson et al., 2002).

Nutz et al. (2018) describe that relatively shallow lake environments with a large fetch for the dominant wind direction, are influenced mostly by a wind-induced lake-scale water circulation and aforementioned wave-related processes. They concluded that water bodies, for which the ratio between the dominant fetch [km] and mean depth [m] (I_{WWB}) is over 3, can be categorized as wind-driven water bodies. These water bodies are characterized by wind-induced surface currents, which go down at the downwind side of the lake, from where they generate a return flow in the lower part of the water column toward the upwind side of the lake. However, usually these lakes are narrow and have a dominant wind direction in longitudinal direction. A lake with irregularly shaped subbasins and an overall complex geometry, like Taihu lake, China, can show an intricate pattern of circulations (Liu et al., 2018). For this very shallow lake (<3 m), wind shear is thought to be an important driver of these circulations and vertical variations are bound to relatively deeper parts of the lake. The morphology of wind-driven water bodies commonly shows shoreface-connected ridges (e.g. longshore, flying or cuspate spits), wave-cut platforms and various cross-shore structures (e.g. surf bars, beach cusps and berms) (Schuster et al., 2005; Ashton et al., 2009).

* Corresponding author.
E-mail address: a.m.ton@tudelft.nl (A.M. Ton).

https://doi.org/10.1016/j.coastaleng.2022.104268
Received 30 June 2022; Received in revised form 27 September 2022; Accepted 15 December 2022
Available online 16 December 2022

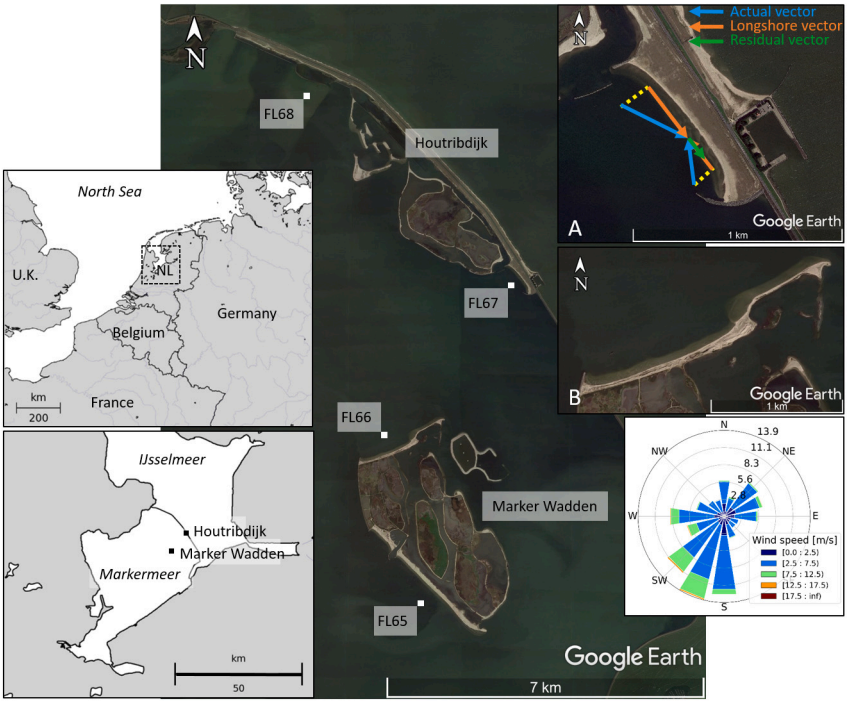

Fig. 1. Overview of measurement locations, where locations FL65 and FL66 mark the measurement locations near respectively the Zuidstrand and Noordstrand of the Marker Wadden and FL67 and FL68 the measurement location on the Markermeer side of the Houtribdijk. Subfigure A shows a top view of the study site near FL67, with a description of calculation residual vector. Subfigure B shows a top view of the study site near FL66. Wind rose of measurement period, 1-2-2019 to 10-2–2021 at KNMI station Lelystad.

Two study sites in lake Markermeer, the Netherlands, provide a unique opportunity to study longshore transport along low-energy, non-tidal beaches. With an I_{WWB} of approximately 10, lake Markermeer classifies as a wind-driven water body. Moreover, some of the sedimentary characteristics are also recognized in lake Markermeer, such as wave-cut platforms (Ton et al., 2021), spits and cusps. These wind-driven hydrodynamics are confirmed by Van Ledden et al. (2006) and Vijverberg (2008), who report that the Markermeer circulation currents are induced by pressure gradients due to wind-driven water level set-up. Besides the vertical circulation, they also describe horizontal components for the Markermeer. The horizontal circulation direction is thought to be related to shallower areas in the lake and other bathymetrical features. This is not specified in the literature, but we hypothesize that in the shallow areas in the north and west of the lake, water level set-up due to wind will be higher than in deeper areas, inducing a flow from shallow to deep. Vertical circulation velocity was estimated to be up to 0.35 m/s during 8 Beaufort wind and horizontal circulation was estimated between 0.1 and 0.2 m/s.

Although both cross-shore and longshore processes have been appointed as drivers for morphological development on low-energy beaches, the importance of either one is not clear. Moreover, the influence of wind driven circulation on longshore currents and transport is thought to be important (Nutz et al., 2018), but is not quantified. When the low-energy beaches have a flood safety function, information on volume losses or gains due to longshore transport is of vital importance for developing an efficient maintenance strategy.

The goal of this research is to explore the nature of the large-scale circulation currents and assess how they affect nearshore longshore currents, relative to the importance of wave-driven currents. Moreover, we want to find out how these longshore currents affect longshore transport and what this implicates for the design of low-energy, non-tidal beaches.

The next section describes the study sites at which nearshore and offshore waves and currents were monitored, together with bathymetrical changes. It further describes the methods, among which the numerical model that was used. Section 3 shows the relation between the currents and morphological development at the first study site and a validation via an application of the model to the second study site. In Section 4 the results are discussed and the paper ends with conclusions in Section 5.

2. Study sites and methods

2.1. Study sites

Lake Markermeer is a shallow (~4 m deep) inland fresh-water lake with regulated water levels between approximately NAP -0.3 m and -0.1 m in summer and around NAP -0.25 m in winter (Rijkswaterstaat, 2018). NAP is the vertical reference datum in the Netherlands, close to mean sea level.

Lake Markermeer is separated from lake IJsselmeer by a dam, the Houtribdijk (Fig. 1). Half of the Houtribdijk was reinforced by artificial sandy foreshores, constructed between 2018 and 2020 (Rijkswaterstaat, 2019). These sandy beaches provide a smooth transition between dike and lake, benefiting biodiversity and water quality in the lake. The first location, near monitoring station FL67, is located at the Houtribdijk on the side of the Markermeer (Fig. 1). This beach is approximately 800 m long, has a D_{50} of 250 μm and is situated between two groynes.

The second site is situated at the north side of the Marker Wadden, located near monitoring station FL66. This artificial archipelago consists of shallow marsh islands, protected by two stretches of sandy beaches and dunes on the north and southwest side and a rubble mound revetment on the west side. The Marker Wadden are meant to improve water quality and ecological habitats in this area. They were constructed between 2016 and 2020 and extensions are still being built (Van Leeuwen et al., 2021). The second site is situated at the northwest side of the Marker Wadden archipelago, constructed since 2016. This beach is approximately 2100 m long in total, and 1400 m in between the dam on the southwesterly side and the "soft edge", the sandy protrusion on the northeasterly side. It was constructed of sand with a D_{50} of 350 μm. The 95-percentile H_{m0} at locations FL67 and FL66 is respectively 0.54 and 0.53 m (Ton et al., 2021).

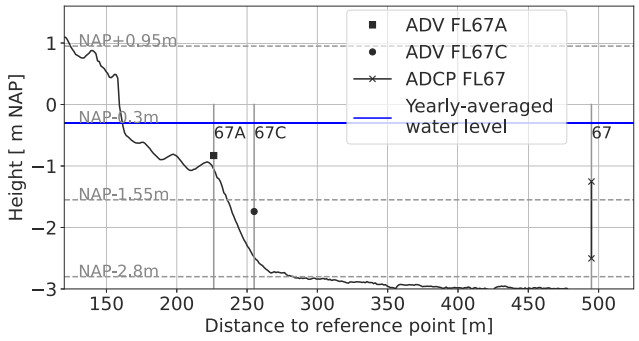

Fig. 2. Overview of measurement locations, where ADV is Acoustic Doppler Velocimeter and ADCP is Acoustic Doppler Current Velocimeter shown on the Houtribdijk cross-shore profile, profile was measured in January 2021.

Generally the profiles of low-energy beaches have a steep foreshore with seaward a low-gradient, subaqueous platform (Jackson et al., 2002). The Markermeer beaches show a similar profile shape, where the platform connects to the deeper lake bed with a steep slope (Ton et al., 2021) (Fig. 2).

2.2. Monitoring

At locations FL65, FL66, FL67 and FL68, approximately 400 m from the shoreline, ADCPs (Acoustic Doppler Current Profilers) were installed at the bed, looking up (Figs. 1 and 2). These ADCPs measured current velocity and direction in layers over the water column. The bed levels at the four locations were NAP-4.50 m, NAP-4.29 m, NAP-2.87 m and NAP-3.52 m respectively, while the year-average water level is around NAP-0.3 m. All ADCPs had a blanking distance of 25 cm, layer sizes of 25 cm and measured with 500 pings per ensemble of 10 min.

At the Houtribdijk site, hydrodynamics were monitored by two ADVs (Acoustic Doppler Velocimeter) positioned in the cross-shore (Fig. 2). The bed levels and heights of the instruments are given in Table 1. The measurement frequency was 8 Hz for both instruments.

At the Houtribdijk, bathymetric data was collected monthly by the contractor between completion in May 2019 and October 2019, after which monitoring was conducted by a survey company between November 2019 and April 2021. At the Marker Wadden, every three months, the bathymetry was monitored. Different equipment was used for bathymetry, shallow bathymetry and topography (Table 2). At the Houtribdijk (HRD), 35 transects were monitored with a spacing of 25 m. At the Marker Wadden (MW), the deep bathymetry and topography was monitored with a high density and the shallow bathymetry in transects. Transects covering the southwesterly 1400 m of the beach with a spacing of 50 m were measured almost every 3 months from October 2019 onwards.

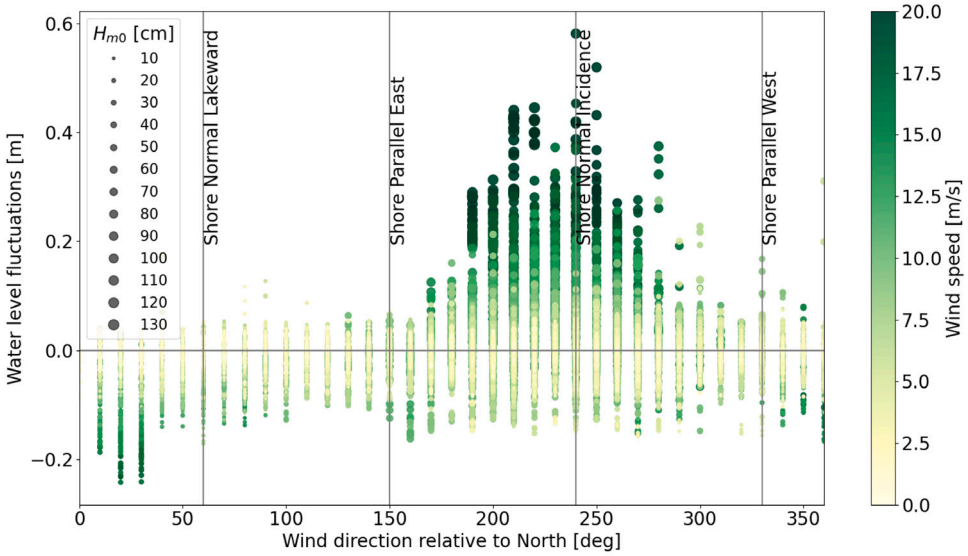

(a) Relation wind, water level fluctuation and wave height based on wave gauge data FL67

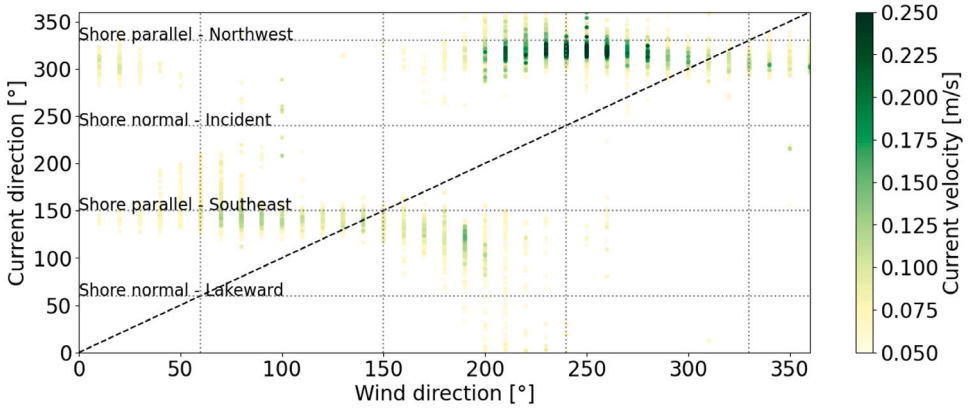

(b) Relation wind to flow direction (coming from), FL67

Fig. 3. Wave, water level and flow characteristics, FL67, March 2019–March 2021.

Table 1
Bed levels and ADV heights averaged over measurement period.

	FL67C	FL67A
Bed level [NAP+m]	−2,51	−1,21
ADV height [NAP+m]	−1,74	−0,83
ADV height above bed [m]	0,77	0,38

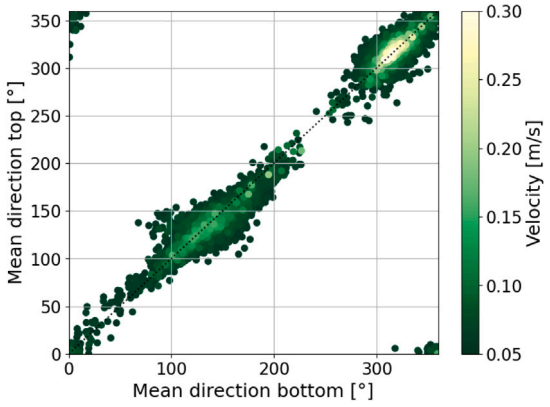

Fig. 4. Relation bottom and top current direction, measured by the ADCP at location FL67.

2.3. Characterization hydrodynamics

The wind climate in the Netherlands is dominated by south-westerly storms (Fig. 1). For our study sites, this dominant wind direction coincides with the largest fetch. Waves are fully determined by local wind and they are depth-limited for the dominant wind direction and fetch-limited for other directions (northwest to southeast) (Fig. 1). The significant wave height (H_{m0}) generally does not exceed 1.5 m and the peak period is typically between 2.5 and 3.5 s during storms. Since the Markermeer is a largely closed off basin, water level fluctuations are mainly caused by wind set-up. For southwesterly wind, location HRD (near FL67) is subjected to a rise in water level and wave height, while for northeasterly wind, a water level set-down and relatively small waves are observed (Fig. 3(a)). The impact of simultaneous high water levels and wave heights on the shape of the cross-shore profile was described by Ton et al. (2021).

The ADV at FL67 shows that currents at this location are bi-directional toward the northwest and southeast, i.e. the longshore direction (Fig. 3(b)). A similar pattern is observed for more nearshore locations FL67C and FL67A. At location FL67C, currents predominantly come from the northwest (63.4%), while at the more nearshore location FL67A, currents are almost equally distributed over the northwest and southeast direction, with a slight predominance for currents coming from the southeast direction (53.2%). From literature we would suspect the current direction to be dependent on the wind direction (Jackson et al., 2002; Nutz et al., 2018), which is confirmed by the measurements (Fig. 3(b)). For wind directions ranging from approximately 40 to 200 degrees, the flow direction at FL67 is toward the northwest, while for wind directions from 200 to 360 and 0 to 40 the flow directions is toward the southeast. The highest current velocities are found for winds ranging from 150 to 280 degrees for all three locations. These are also the directions with the strongest winds.

For more insight into the circulation patterns that are driven by the described water level set-up and down, the ADCP measurements are analyzed. The ADCP measurements at locations FL65, FL66, FL67 and FL68 show no significant differences between the velocities and directions of the current in the top half of the water column and the bottom half (Fig. 4). Concluding, the large-scale circulations in lake Markermeer are mostly horizontal.

2.4. Modeling

2.4.1. Model setup

To extend our knowledge of the hydrodynamics around our study sites, we used a numerical model, Delft3D (Deltares, 2018). By using a model that includes the complete Markermeer, we can obtain insight into large-scale circulation currents. Moreover, the individual forcing of waves and currents can be researched.

Our model is based on the suspended sediment model of the Markermeer, as developed by Van Kessel et al. (2008). Only the WAVE and FLOW module were adopted from this model. We use the model depth-averaged, since currents in our area of interest are uniform over depth (Fig. 4) and included Coriolis forcing. The original model has a grid cell size of approximately 150 m in our area of interest, which is not detailed enough for our application. Therefore, the northeastern corner of the model was nested in the original model (Fig. 5). This nested grid is refined by a factor 9 in both directions and refined more along the southwestern beach of the Marker Wadden (FL65) and at the Houtribdijk (FL67). This nest has two new, open boundaries.

2.4.2. Model validation

Waves, water levels and flows are validated with measurements from locations FL65, FL66, FL67, FL67C, FL67A and FL68 for two periods (Fig. 1). The first period is from February 7 to February 13, 2020, during which storm Ciara passed. During storm Ciara, the peak wind speed was around 23 m/s at lake Markermeer, and the wind direction was south to southwest. The second period lasts from June 1 to June 9, 2020, which is a calm period. During this period the maximum wind speed was around 15 m/s and directions varied from north to southwest.

Wave heights are somewhat overestimated by the model, especially at locations FL67, FL67C and FL67A, and modeled peaks have a slightly longer duration than measured peaks (Figs. 6(a) and 6(b)). Measured and modeled wave directions correspond very well during all periods. Water levels are well-simulated by the model, peaking at the right moment and the right level for location FL68, Fl66 and FL65, with just a slight underestimation at locations FL67, FL67C and FL67A. Flow velocities are reproduced well by the model at locations FL65, FL66, FL67 and FL68. At the nearshore locations FL67A and FL67C, where one or more (horizontal) circulation cells are present under certain conditions, the model results deviate slightly more. Since we are looking at just one point measurement, the exact location(s) of these cell(s) can make a big difference. However, at all locations, flow directions match the measurements, apart from slight deviations around the tipping points. When incoming wind varies around the shore normal, longshore flow can switch 180°, which we call a flow reversal point. The flow reversal points and comparison between measurements and model are also visible in Fig. 13.

Above descriptions are reflected in the root mean squared errors (RMSE) (Table 3). Although in general peaks and absolute values are close, the RMSE can be somewhat inflated, especially for the flow direction. The RMSE indicator specifically tends to exaggerate the larger deviations that occur at small flow velocities. Meanwhile, during moments of higher flow velocities when current are well-developed, deviations are smaller.

2.5. Calculation longshore current and transport

With the flow measurements and bathymetrical surveys at location HRD, current characteristics per morphological period are defined. The morphological period is the period between two surveys, which is approximately 1 month in winter and 2 months in summer. The continuously measured current vector is reduced to a 10-min rolling mean and then translated to a number proportional to sediment transport with Eqs. (1) and (2) (Bosboom and Stive, 2021):

$$\langle S_b \rangle \propto \langle u|u|^2 \rangle, \tag{1}$$

Table 2
Measurement equipment used for bathymetry, shallow bathymetry and topography at different locations with vertical accuracy between brackets.

	Houtribdijk (FL67)		Marker Wadden (FL66)
	May 2019–October 2019	*November 2019–April 2021*	*July 2018–present*
Bathymetry	Singlebeam (±0.1 m)	PingDSP (±0.1 m)	Multibeam (±0.2 m)
Shallow bathymetry	RTK-GNSS carrier (±0.03 m)[a]	RTK-GNSS carrier[a]	RTK-GNSS carrier[a]
Topography	RTK-GNSS carrier[a]	LiDAR drone (±0.05 m)	Structure-from-motion with drone (±0.05 m)

[a]Accuracy of all RTK-GNSS carriers is equal.

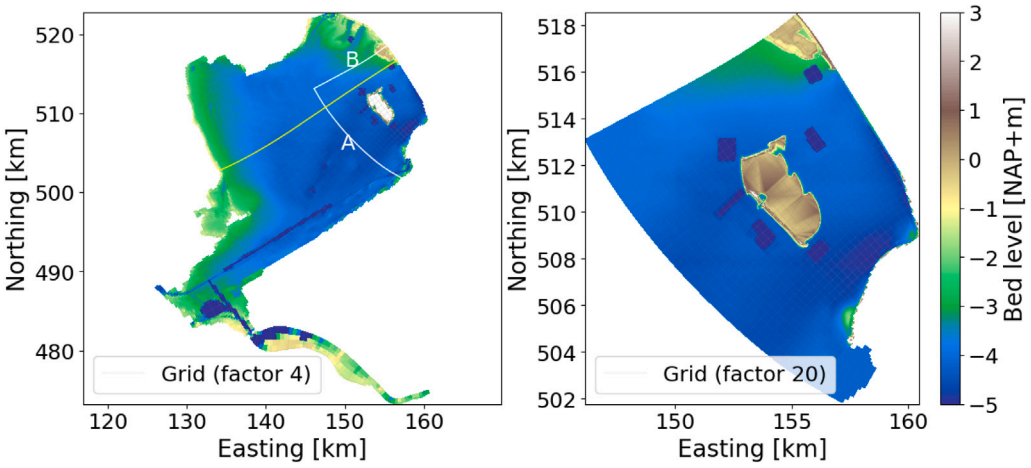

Fig. 5. Left: The total Markermeer grid with bathymetry and the boundaries for the nested model. Boundary A is a water level boundary and boundary B is a flow boundary. Wave spectra are imposed on both boundaries. Right: The nested grid and bathymetry, in which six sand mining pits are visible (±40 m deep). The yellow line indicates a later described cross-section through FL67.

Table 3
RMSE of model versus ADV measurements of significant wave height (H_{m0} [m]), water level (h [m]), flow velocity (u_{vel} [m/s]) and flow direction (u_{dir} [°]).

	FL67	FL67C	FL67A
H_{m0}	0.229	0.178	0.321
h	0.042	0.070	0.070
u_{vel}	0.032	0.083	0.073
u_{dir}	54.1	60.7	57.5

Table 4
Vertical morphological sections.

	Name section	Upper boundary	Lower boundary
I	Beach face section	NAP+0.95 m	NAP-0.3 m
II	Platform section	NAP-0.3 m	NAP-1.55 m
III	Offshore section	NAP-1.55 m	NAP-2.8 m/NAP-4.2 m[a]

[a]Respectively FL67 and FL66.

$$\langle S_s \rangle \propto \langle u|u|^3 \rangle, \tag{2}$$

where S_b is bed load transport, S_s is suspended load transport and u is flow. Both bed load transport and suspended load transport are considered for the transport vector. This vector is projected on the coastline, as a longshore vector (Fig. 1). The residual transport capacity based on current measurements for the morphological period is then calculated with the mean of the longshore transport vector, averaged over all 10-minute periods in the morphological period (hereafter referred to as $S_{b\,or\,s,long,net}$).

Based on the bathymetrical surveys, the actual volume flux can be estimated. We do this by calculating the volumes of different vertical sections separated by four vertical levels (Fig. 2):

- above the beach face (NAP +0.95 m),
- the annual mean lake level (NAP-0.3 m),
- the submerged slope, just below the platform (NAP-1.55 m),
- just below the lake bottom (HRD: NAP-2.8 m, MW: NAP-4.2 m).

In between these levels, three sections are defined: the beach face section, the platform section and the offshore section (Table 4).

The first and second vertical zones (I, II) are equal in height, as is the third vertical zone for location HRD (Table 4). Because the offshore Markermeer bed level is deeper at location MW, the bottom level is lower over there. To analyze longshore sediment transport, the beach is divided into two horizontal sections. For location HRD this is the northwestern section, between transect 60.55 and 60.925, and the southeastern section, between transect 60.925 and 61.3 (Fig. 10). Both sections are 350 m wide. Per morphological period, the change in volume over time for each vertical section and horizontal section is calculated with $Q_{sed} = \Delta V / \Delta t$ in m^3/day.

3. Results

3.1. Lake circulations

3.1.1. Large-scale

The large-scale lake circulations are thought to be related to differences in water level set-up due to bathymetrical variability (Van Ledden et al., 2006; Vijverberg, 2008). The ADCP measurements showed that these currents are uniform over depth, and thus they are classified as horizontal.

The numerical model is fit to test the relation between set-up and currents. For southwesterly wind, indeed a higher water level set-up is found in the shallow areas in the north of the lake (Fig. 7(a)). The set-up difference at the leeward shore, the Houtribdijk, induces a flow from shallow to deep. Therefore,the large-scale clockwise circulation occurs for these conditions (Figs. 7(a) and 8). From southerly and westerly wind, a similar pattern occurs. For wind from the east, one large cell circulates counter-clockwise (Fig. 7(b)). This can be explained following the same principle. Model runs without these shallow areas,

(a) Location FL67

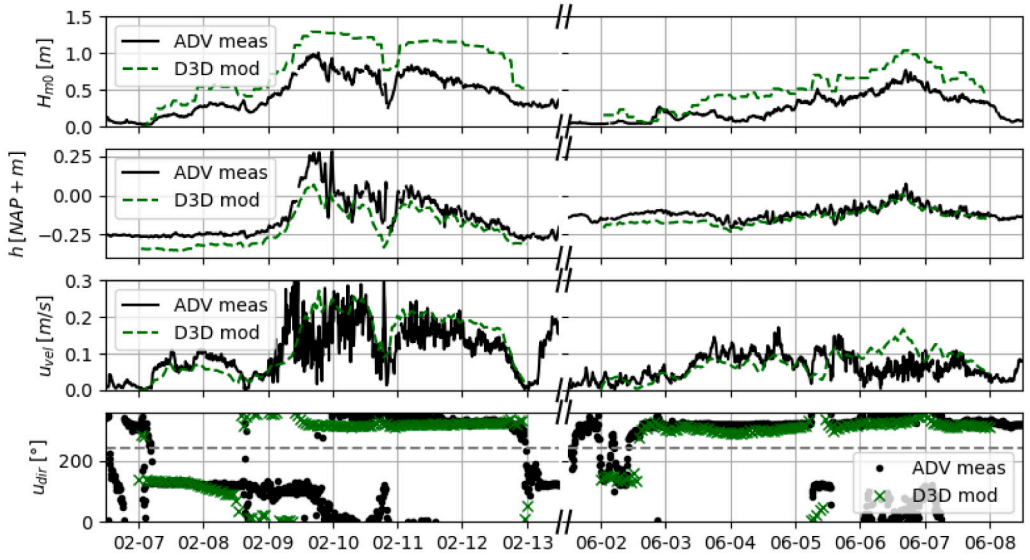

(b) Location FL67A

Fig. 6. Validation of model results to ADV measurements of significant wave height (H_{m0} [m]), water level (h [m]), flow velocity (u_{vel} [m/s]) and flow direction (u_{dir} [°])

but with a uniform depth, show very little large-scale circulation. This affirms our hypothesis. For both winds from the southwest and east, flow converges between the area northeast of the Marker Wadden, causing an acceleration in this area. For wind from the north, multiple circulation cells form, showing less distinct patterns, especially in the area around the Marker Wadden and FL67.

3.1.2. Nearshore

The large-scale currents are expected to influence the nearshore currents at the study sites. At the Houtribdijk beach two characteristic flow patterns can be distinguished. In the first situation, for wind from the west, we have uniform flow in the nearshore between the groynes (Fig. 8(c)). In the second and most common situation, for wind from the south to southwest, a counterclockwise circulation cell occurs between the groynes, where flow at location FL67C and further offshore is toward the southeast, while at location FL67A and further nearshore it is toward the northwest (Figs. 8(a) and 8(b)). The presence of a circulation cell at the Houtribdijk beach explains difference in the occurrence of flow directions that were measured at FL67A (nearshore) and FL67C (more offshore) (Section 2.3). Especially for winds from the southwest to west, the offshore flows (around FL67) reach the nearshore. These offshore flows are part of the large-scale circulation, as they coincide with flows in the northwest region of the lake (Fig. 7(a)). Moreover, since waves do not break around FL67, we can assume that the offshore flows are directly related to the large-scale lake circulations. Lastly, we would not expect significant wave-driven longshore currents, since waves are nearly normally incidence for southwesterly wind.

Bathymetry-induced differences in water level set-up cause large-scale, horizontal circulations. These circulations reach and influence the nearshore currents, as do local geometric features.

3.2. Influence large-scale circulation and wave-driven flow

We hypothesized that the influence of the large-scale, wind-driven circulations on the longshore transport is significant. To quantify the influence of wave-driven currents, the numerical model with and without waves included is compared for a range of wind conditions. At

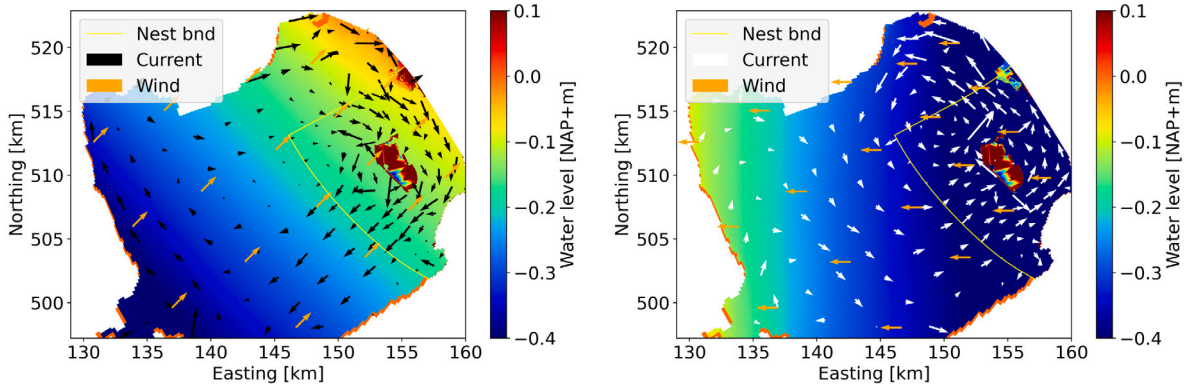

(a) Water level for schematic model with 15 m/s wind from 225°(orange vectors), with flow (black vectors)

(b) Water level for schematic model with 15 m/s wind from 90°(orange vectors), with flow (white vectors)

Fig. 7. Top view water levels and currents from Delft3D model.

location FL67A, the currents with and without waves point mostly toward the same direction for all wind conditions (Fig. 9(a)), but differ in magnitude. At the more offshore location FL67C, currents with and without waves differ in direction for winds coming from 157.5° to 202.5° (Fig. 9(b)). This difference is caused by the waves "pressing" the circulation cell against the beach for these wind directions, thus changing the current direction specifically at location FL67C. Blue colors indicate that the modeled current with waves included is larger and red colors the opposite. The average difference in magnitude between including or excluding waves are 0.01 m/s for both locations, but the differences vary per wind condition (Fig. 9). For most wind conditions and at both locations, nearshore flow velocity is decreased when waves are included in the model. The decrease can vary up to 0.1 m/s. For southwesterly wind, flow velocity is increased by waves at both locations. This is caused by the water level set-up in the northwest of the lake during these conditions. This set-up is enhanced by the waves, increasing also the offshore current in front of the beach, toward the southwest (Fig. 8(b)). This "offshore" flow counteracts the nearshore flow toward the northeast, decreasing the flow with waves more than without waves. This velocity increase by waves is therefore not related to obliquely incident waves, but the effect of waves on the large-scale lake circulations. To conclude, large-scale circulation flow is a major component of the nearshore current, compared to the wave-driven current. Both components can enhance each other and oppose each other, depending on the wind direction.

3.3. Morphology

The morphology of the Houtribdijk beach is analyzed, to be able to link currents to volume fluxes. A clear erosion and accretion pattern is visible at the Houtribdijk beach (Fig. 10). Most erosion takes place around the beach face and the platform over a period of 21 months. Sedimentation takes place in the offshore section, for the most part toward the groyne on the northwest side (between −850 m to −600 m in Fig. 10). Although we see a strong net pattern over this long period, sedimentation and erosion do vary over time (Fig. 11). The northwestern (NW) beach face and the southeastern (SE) beach face erode at a similar pace, apart from two periods. After construction in May 2019 and around March 2020, the NW beach face eroded greatly, while the SE beach face only eroded slightly. Apart from a few moments, the platform also shows a decreasing trend. Right after construction, a quick decrease of the platform volume is also visible, suggesting an adjustment effect for both the beach face and platform toward the natural profile shape (Ton et al., 2021). The offshore volumes grow more steadily over time, showing a greater increase on the NW, as described above. Most volume fluctuations take place during the storm season, from October to April.

Morphological development shows clear signs of cross-shore transport at the beach face and longshore transport in the platform and offshore section.

3.4. Relation hydrodynamics and morphology

We hypothesized that $S_{b\,or\,s,long,net}$, based on (measured) longshore currents, is related to the longshore volume flux, based on difference in volumes of the NW-section and SE-section. To test the hypothesis, $S_{b,long,net}$ calculated from FL67A (nearshore) and FL67C (more offshore) are plotted against the volume changes (Q_{sed}) of the beach face section, platform section and offshore section (Fig. 12). These results are compared to the results for $S_{s,long,net}$ later, based on R^2. In this figure, positive values for both the transport capacity and volume flux indicate transport toward the northwest, while negative values indicate transport toward the southeast.

For FL67A the fitted lines nearly cross (0,0), indicating that a positive $S_{b,long,net}$, toward the northwest, coincides with a positive Q_{sed}, toward the northwest (Fig. 12). All $S_{b,long,net}$ values for FL67C are negative, which means toward the southeast and it is impossible for the fitted lines to cross (0,0). For this location we see a negative Q_{sed} (toward the southeast) for more negative values of $S_{b,long,net}$ and positive Q_{sed} (toward the northwest) for less negative values of $S_{b,long,net}$.

Both locations differ in range of $S_{b,long,net}$. Since FL67A is more nearshore and at a more shallow location (Table 1), flow velocities are higher and more varied at this location. $S_{b,long,net}$ for the total period is small compared to the shorter periods. This indicates little net transport from NW to SE and vice versa. However, measurements show that not all gross transport comes back when deposited (Fig. 10).

For the beach face, there is no significant relation between $S_{b,long,net}$ and Q_{sed} for both locations (Table 5, Figs. 12(a) and 12(b)). This implies that (solely) current-driven transports cannot explain the volume changes of the beach face. For the platform and offshore, the relation is more pronounced (Figs. 12(c), 12(d), 12(e) and 12(f)). Despite the location of FL67A closer to the platform than FL67C, the relation for FL67A and the platform section is less significant. And although the location of FL67C is closer to the offshore section than FL67A, the relation for FL67C and the offshore section is less distinct.

Both the relations between $S_{b,long,net}$ and Q_{sed} and between $S_{s,long,net}$ and Q_{sed} are significant for the platform and offshore section (Table 5). However, the relation for $S_{b,long,net}$ is stronger, especially for location FL67A. This indicates that morphological development at the platform and offshore section is driven by longshore currents in the nearshore and that bed load transport is likely to be more prevalent than suspended load transport at the platform.

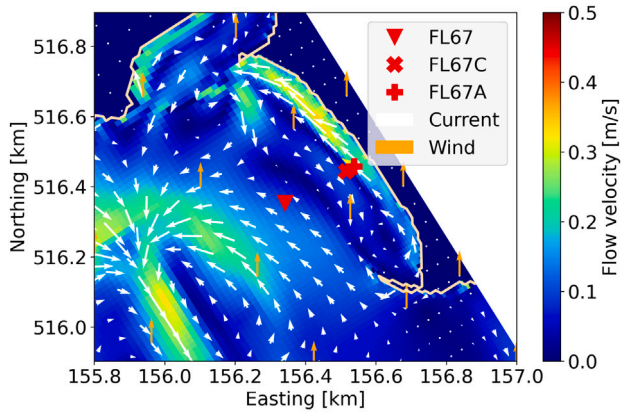

(a) Flows for schematic model with 15 m/s wind from 180°.

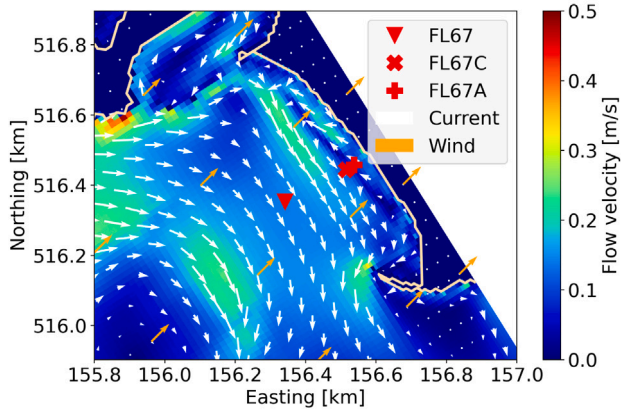

(b) Flows for schematic model with 15 m/s wind from 225°.

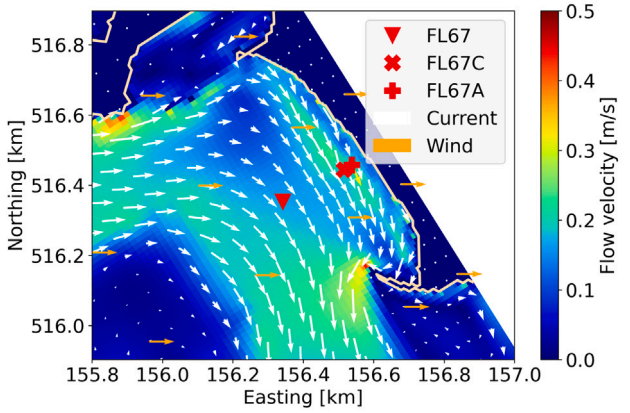

(c) Flows for schematic model with 15 m/s wind from 270°.

Fig. 8. Top view of flows from schematic Delft3D model, with wind in orange vectors and flow in white vectors.

Table 5
R^2 relation $S_{b,long,net}$ or $S_{s,long,net}$ and Q_{sed}.

	Beach face	Platform	Offshore
FL67A - S_b	0.35	0.76	0.86
FL67A - S_s	0.24	0.44	0.81
FL67C - S_b	−0.08	0.85	0.54
FL67C - S_s	−0.07	0.88	0.55

3.5. Prediction longshore transport

Since $S_{b,long,net}$ and Q_{sed} are related for the platform and offshore section, the numerical hydrodynamic model can be used to predict direction and magnitude of the volume flux. To do so, we follow these steps:

1. Choose a range of wind conditions, i.e. combinations of wind direction and wind velocity.
2. Predict the flow direction and magnitude per wind condition with a numerical model with waves and flow.
3. Convert the predicted flow into $S_{b,long,net}$.
4. Calculate the occurrence of every wind condition.
5. Combine the predicted potential transports and wind statistics, to find the total net transport capacity, $S_{b,long,net,tot}$.

From this we can learn the net volume flux direction for a certain period or a long-term mean value, if the wind statistics are based on a long enough period.

The directions and magnitudes of the predicted nearshore flow correspond well with the measurements for both locations (Fig. 13). Most inaccuracies are found for the wind conditions near the flow reversal point for which the currents change direction. For FL67A this is around 202.5° and for FL67C around 180°. The predicted velocities for these scenarios are smaller than the measured velocities and the direction is less distinctly toward the northwest for southerly wind directions.

$S_{b,long,net}$ is calculated for all wind conditions by combining the flows to the third power (Eq. (1)) with the occurrence of these scenarios over the measurement period (June 2019–February 2021). For location FL67A the measured flows toward the northwest and southeast almost cancel each other out, resulting in a southwesterly directed transport capacity (i.e. offshore). The predicted flows for this location result in a southerly directed transport capacity. The measured and predicted residual transport capacities for FL67C are both toward the southeast, although differing somewhat in magnitude. The longshore component of the modeled residual transport capacity are visualized with the relation between transport and actual flux (Fig. 12, dotted and dash-dotted lines). The total transport capacity is small compared to the values per morphological period (Fig. 12).

3.6. Implications to design - Marker Wadden

The study site at the Marker Wadden is used to test whether a prediction based on flow vectors can help to predict volume flux direction at a location with no nearshore measurement. This study site lies under an angle relative to the most common southwesterly winds, so a distinct signal is expected compared to the study site at the Houtribdijk.

3.6.1. Longshore current

At the Marker Wadden, a circulation cell is present for southwesterly wind, similar to the one at the Houtribdijk site (Fig. 14(a)). More offshore, the flow is directed toward the southwest, while it is directed toward the northeast in the nearshore.

We analyzed the nearshore data for multiple wind conditions at a similar water depth as FL67A, approximately 1 m, and named it FL66A (Fig. 14(a)). At this location, also two flow reversal points for flow direction were visible but at different wind angles, around 157.5° and 337.5° (Fig. 14(b)). From winds from the south to northwest, nearly alongshore flows toward the northeast are predicted and for opposite winds opposite flows. The average difference in current magnitude when including and excluding waves from the model is 0.01 m/s, the same number as for location FL67A and FL67C. The waves affect the currents in two manners. The first is visible for winds between the southwest and west, for which flows from the model without waves are stronger. This is caused by the water level set-up in the northwest

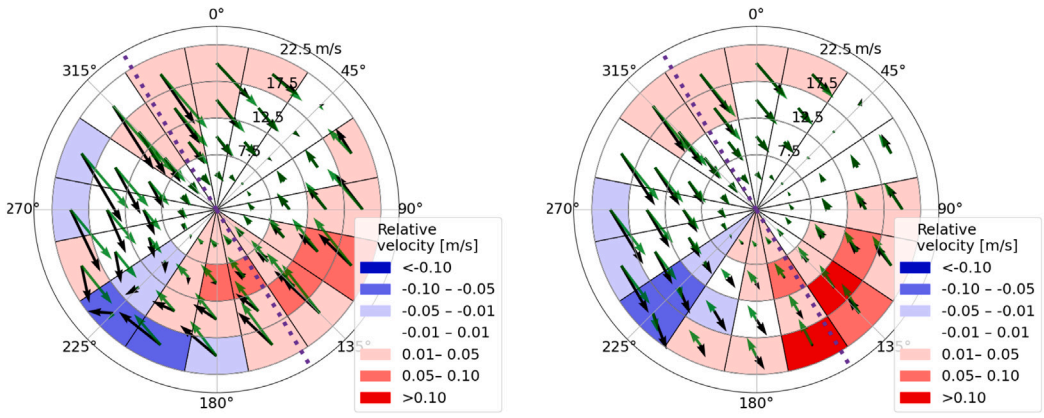

(a) Location FL67A (b) Location FL67C

Fig. 9. Equilibrium currents from numerical model runs with waves (black vectors) and without waves (green vectors) for corresponding wind direction and velocity and difference in velocity (no waves-waves, colored). Shoreline orientation (purple dashed line). Example: The most upper vector gives the equilibrium flow for the model run with northerly wind (0°) at 20 m/s.

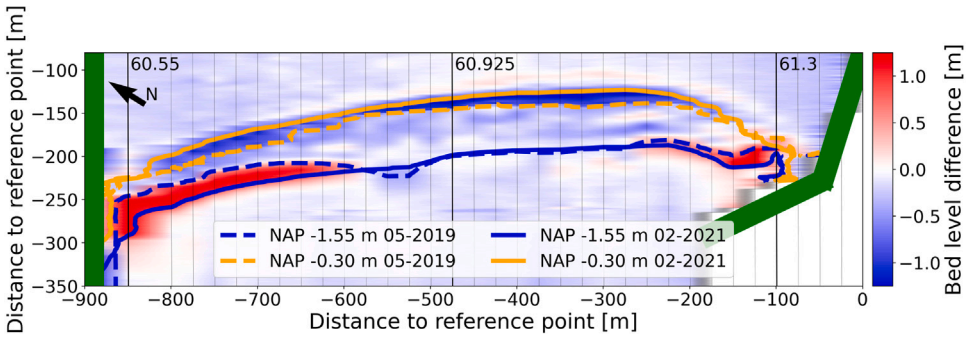

Fig. 10. Morphological development location FL67 between as built, May 2019, and February 2021. Groynes in green.

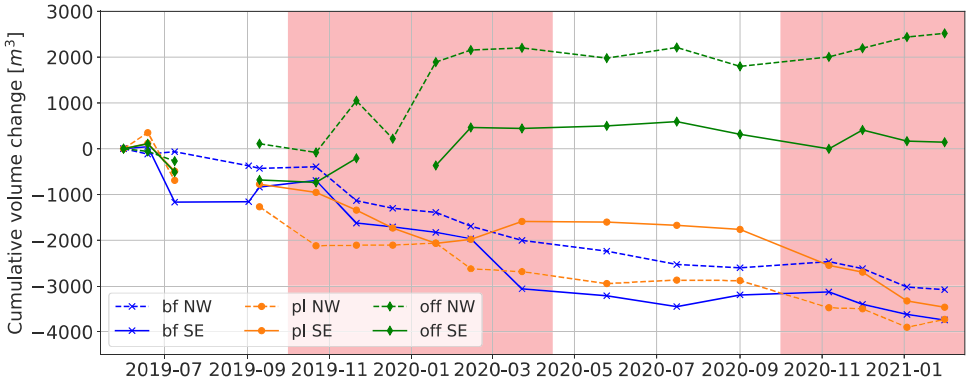

Fig. 11. Volumes north-west (dashed) and south-east (solid) of transect 69.925 in beach face (bf), platform (pl) and offshore (off). Storm seasons are colored red.

of the lake during these conditions. This set-up is enhanced by the waves, increasing also the return current in front of the beach, toward the southwest (Figs. 8 and 14(a)). This "offshore" flow counteracts the nearshore flow toward the northeast, decreasing the flow with waves more than without waves. This velocity decrease by waves is not related to obliquely incident waves, but the effect of waves on the large-scale lake circulations. For winds between the northwest and northeast, especially for higher wind velocities, the second process is visible and we see that waves do reach the nearshore and amplify the longshore current. Moreover, we see more offshore directed flows for shore normal winds in the model with waves. Concluding, the effect of waves on longshore currents depends on the wind direction and is low on average.

3.6.2. Model prediction

For the prediction of longshore transport, we studied a short period from April 2019 to July 2019. Since winds from the southwest are dominant during this period, the $S_{b,long,net,tot}$ is toward the east with a magnitude of $2.1 * 10^{-2}$ $(m/s)^3$ (Fig. 14(b)). Over this period, the south-western part of the study site loses sediment at the beach face and the platform, while the northeastern part loses less or even gains sediment (Table 6, Fig. 15). This shows sediment transport from southwest to

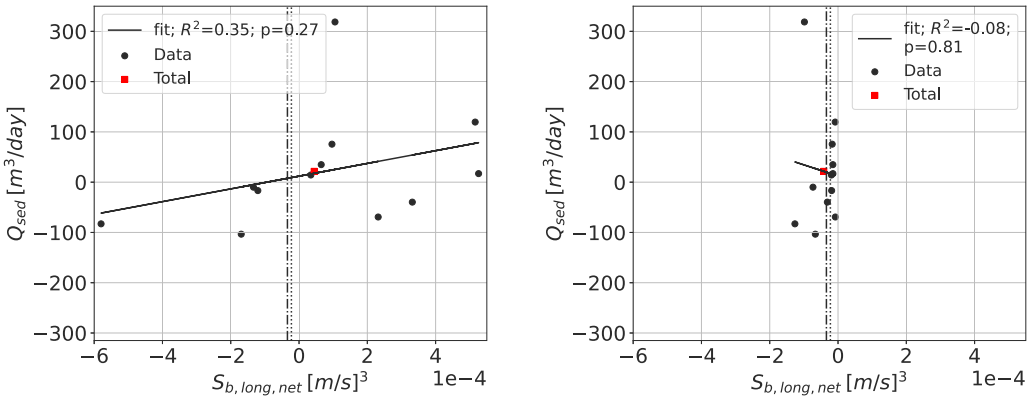

(a) Location FL67A, beach face section.

(b) Location FL67C, beach face section.

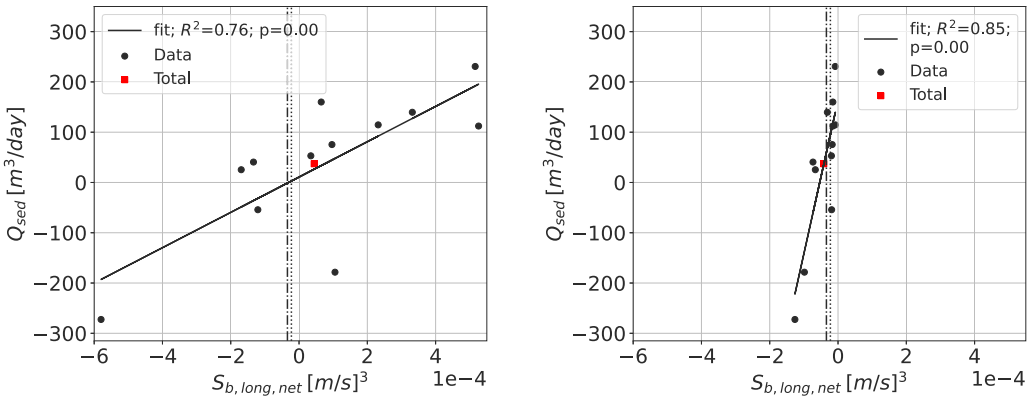

(c) Location FL67A, platform section.

(d) Location FL67C, platform section.

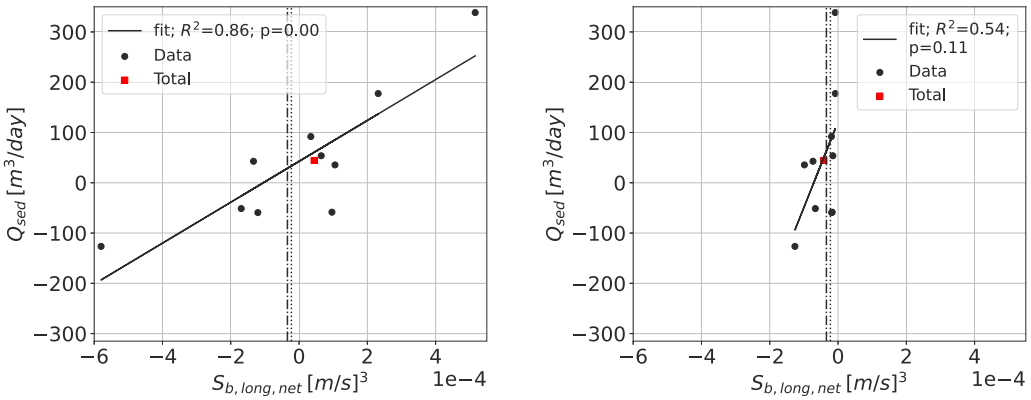

(e) Location FL67A, offshore section.

(f) Location FL67C, offshore section.

Fig. 12. Relation residual transport capacity based on current measurements with actual volume flux from named measurement location and vertical volume section. Dotted line indicates residual transport capacity for the whole measurement period (June 2019–February 2021) for FL67A and dash-dotted line for FL67C.

northeast, which is the same direction as $S_{b,long,net}$. The morphological development of the Marker Wadden beach is only coherent when taking the circulation cell and thus the impact of the large-scale currents into account. Without these, the erosion seen in the lee of the dam was not expected.

To conclude, knowledge of large-scale currents are important for understanding morphological development of the Marker Wadden beach, and have significant impact on the design and maintenance.

Table 6
Volume changes between April and July 2019, for the southwestern and northeastern part of the beach and the vertical sections in m^3, over the 500 m wide sections.

	Beach face	Platform	Offshore
Southwest	−888	−1.385	46
Northeast	−138	42	280
Net	−750	−1427	234

4. Discussion

As was stated in the introduction, different studies expect for this type of water body to have three-dimensional flows, with a return current flowing opposite to the dominant fetch (Van Ledden et al., 2006; Vijverberg, 2008; Nutz et al., 2018). Our measurements do not show this type of flow, but indicate a two-dimensional pattern with horizontal return current. The ADCP's monitor approximately 78% to 93% of the water column, taking into account the blanking distance (0.25 m) and varying upper wave region. Since flows are uniform in

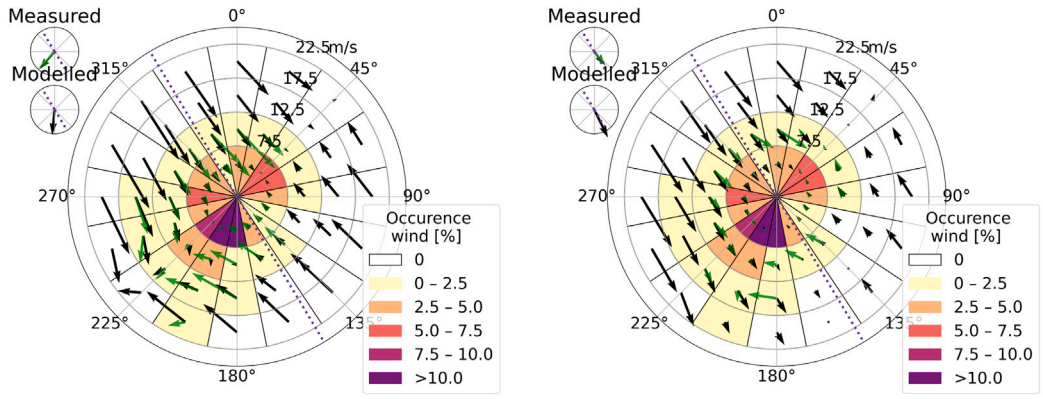

(a) Location FL67A (b) Location FL67C

Fig. 13. Center: Flows measured at measurement location (green vectors) and equilibrium current direction from numerical model runs at same location (black vectors) for corresponding wind direction and velocity and wind statistics (colored). Shoreline orientation (purple dashed line). Top left: $S_{b,long,net}$ for 10-year period, taking only measured wind conditions into account.

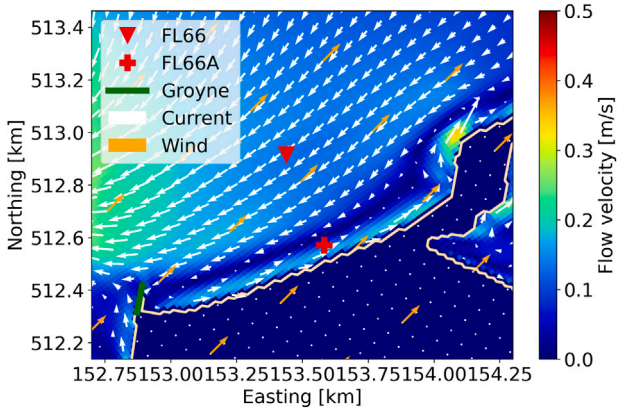

(a) Flows for schematic model with 15 m/s wind from 225°.

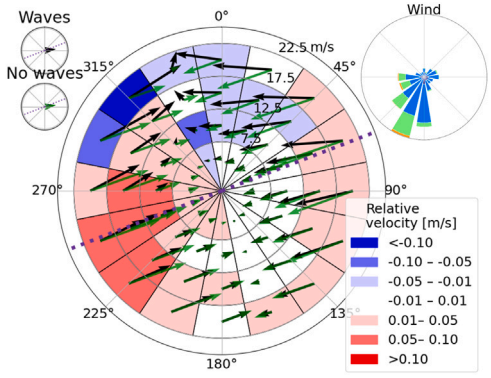

(b) Center: Equilibrium current direction from numerical model runs at nearshore Marker Wadden beach with waves (black vectors) and without waves (green vectors) for corresponding wind direction and velocity and difference in velocity (no waves-waves, colored). Shoreline orientation (purple dashed line). Top left: weighted net transport capacity for period from October 2019 to April 2020. Top right: Wind rose for period October 2019 to April 2020.

Fig. 14. Flows from Delft3D at Noordstrand, Marker Wadden.

this part of the water column, we have no reason to assume 3D flow patterns in our region of interest. The water bodies analyzed by Nutz et al. (2018) range from a depth of 6 m and 30 km fetch to hundreds of meters deep and hundreds of kilometers wide. Lakes as shallow and wide as lake Markermeer were not taken into account. The shallow lake researched by Liu et al. (2018) also shows three-dimensional currents, but dedicates that to a complex bathymetry. The relatively uniform but shallow bed level of lake Markermeer, could explain the lack of observations of vertical return currents.

The model validation shows good agreement between the model results and the ADV measurements. However, the significant wave height is somewhat overestimated by the model. For conclusions on the relative impact of large-scale currents and wave-driven currents on the total longshore currents, this would be a conservative choice in favor of the wave-driven current. Yet the influence large-scale currents is high and thus might be even higher in practice.

For the calculation of $S_{b,long,net}$, we assumed bed load transport, since ripples were observed in the nearshore at all locations and throughout all seasons. A sensitivity analysis showed that with this assumption, the best relation between $S_{b,long,net}$ and Q_{sed} was found. This might be specific for the lake Markermeer beaches.

Relations between $S_{b,long,net}$ and Q_{sed} for the platform and offshore section were found to be significant, but the development of the beach face section cannot be related to this flow-based parameter. Ton et al. (2021) describe that the sediment transport at the beach face is primarily in the cross-shore direction, and that eroded sediment only travels in the cross-shore and longshore direction once it reaches the platform. These results imply that wave action is dominant over current-driven transports for development of the beach face.

The orientation of the Houtribdijk beach, almost perpendicular to the most common southwesterly storms, makes it difficult to predict to which direction the net longshore transport will be. Firstly, because $S_{b,long,net}$ calculated per period is not as strong compared to a beach under an angle such as the Marker Wadden beach. And secondly, because $S_{b,long,net,tot}$ and $Q_{sed,tot}$ are close to zero (Fig. 12). $S_{b,long,net}$, based on flow measurements at the Houtribdijk beach, is slightly positive, indicating net transport toward the northwest, while $S_{b,long,net}$ from the model is slightly negative, indicating the opposite. Since both values are very close to zero, this confirms the sensitivity to minor changes in forcing of a beach under this angle once more. It is favorable for the beach to approach a net zero longshore volume flux on the long term in terms of maintenance. However, we do see longshore transport reflected in the sedimentation spots near the dams (Fig. 10). We observe that sediment that has settled near the dams, does not come back toward the middle of the beach. This is because

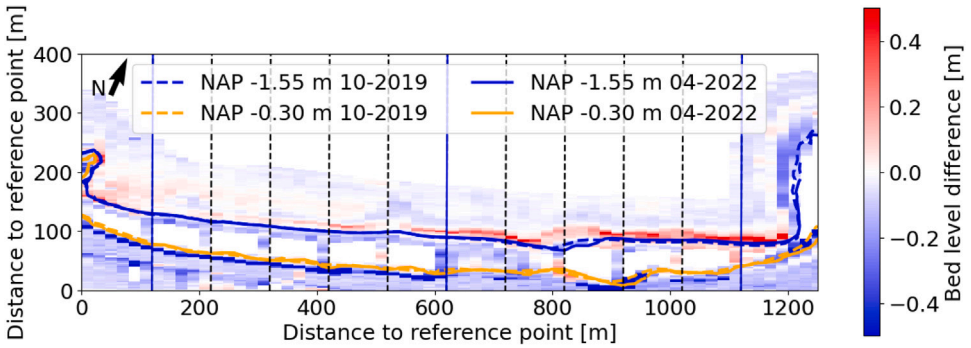

Fig. 15. Morphological development Marker Wadden beach between October 2019 and April 2020. Southwestern section on the left, between the blue transects and northeastern section on the right.

most of the sediment settles below the depth of closure (Ton et al., 2021). So even though net sediment transport is close to zero, the middle of the beach is net eroding. The Marker Wadden beach has a different orientation, which makes the prediction more distinctly to one direction and an $S_{b,long,net}$ of $O10^{-2}$ instead of $O10^{-4}$ at the Houtribdijk. Since the dominant southwesterly storms coincide with a transport capacity direction toward the northeast, a flux toward the northeast is no surprise.

The Marker Wadden beach is a great example where taking into account the large-scale circulations, gives insight into morphodynamic processes. Based on just wave-driven longshore currents, some transport toward the northeast was expected given the dominance of southwesterly winds. The groyne in the southwest was expected to create a lee and retain sediment (Fig. 14(a)). However, this groyne turns out to reverse the offshore flow, making the "lee-side" of the groyne especially vulnerable for erosion (Fig. 15). This affirms that insight into large-scale circulations is crucial for understanding longshore flow in this case.

The development of the Delft3D model, in addition to the field measurements, was crucial in gathering information on circulating flows. This model was essential in understanding the system. With the new knowledge on the importance of large- and small-scale circulations for morphodynamics of lake beaches, adapted field measurements could be done, to make the model less essential. With opposite reasoning, a complex numerical model could replace the need for measurements in similar systems. However, the combination of measurements and model has many added benefits compared to using either one.

5. Conclusion

The goal of this research was to find what causes the described large-scale lake circulations and how these influence nearshore, longshore currents compared to wave-driven currents. Furthermore, to determine how these longshore currents affect longshore transport and its implication on the design of low-energy, non-tidal beaches. Lake Markermeer is characterized as a shallow, wind-driven water body. ADCP and ADV measurements show flows that are nearly uniform over depth, and that flow directions are closely related to wind directions.

To gain more spatial insight into large-scale circulations, a depth-averaged Delft3D model was set up and validated to the measured waves, water levels and currents. This model showed that bathymetry induced differences in water level set-up cause large-scale, horizontal circulations. These circulations affect the nearshore currents greatly, and are dominant over wave-driven longshore currents for most wind conditions regarding nearshore sediment transport. Local geometric features, such as groynes, also influence the flow, inducing smaller scale nearshore circulation cells under distinct conditions.

Longshore volume and coastline changes were measured through monthly bathymetric surveys. Based on flow measurements, sediment transport capacity ($S_{b,long,net}$) was calculated and linked to volume flux (Q_{sed}). A significant relation was found between $S_{b,long,net}$ and Q_{sed} for the full cross-shore profile, except the steep beach face. Through this relation longshore sediment flux can be predicted with model derived flow parameters for a variety of wind conditions, accounting for the complexity of flow circulation patterns discussed above. This is evaluated for a second study site, where we confirmed that the predicted $S_{b,long,net}$ can be a good indicator for longshore volume flux. Moreover, this study site shows that insight into large-scale currents is essential for understanding morphological development, and are a key element to take into account for design an maintenance of sandy beaches in low-energy environments.

Concluding, large-scale circulations are of vital importance for morphological development of low-energy, non-tidal beaches in shallow, wind-driven water bodies.

CRediT authorship contribution statement

Anne M. Ton: Conceptualization, Methodology, Writing – original draft, Writing – review & editing. **Vincent Vuik:** Conceptualization, Methodology, Supervision. **Stefan G.J. Aarninkhof:** Conceptualization, Supervision.

Declaration of competing interest

The authors declare that they have no known competing financial interests or personal relationships that could have appeared to influence the work reported in this paper.

Data availability

Measurement data is available at: https://waterinfo-extra.rws.nl/projecten/@205186/houtribdijk/.

Acknowledgments

This research is part of the LakeSIDE project, which is funded by Rijkswaterstaat, The Netherlands. We want to thank Rijkswaterstaat Centrale Informatievoorziening for guiding and executing the (hydrodynamic) monitoring campaign. Shore Monitoring and Combinatie Houtribdijk are acknowledged for carrying out the morphological surveys at the Houtribdijk. We thank Boskalis Nederland for sharing their bathymetric and topographic data of the Marker Wadden. Finally, we like to thank graduate student Fleur Wellen for her work at the Noordstrand, Marker Wadden.

References

Ashton, A.D., Murray, A.B., Littlewood, R., Lewis, D.A., Hong, P., 2009. Fetch-limited self-organization of elongate water bodies. Geology 37 (2), 187–190. http://dx.doi.org/10.1130/G25299A.1.

Bosboom, J., Stive, M.J., 2021. Coastal Dynamics, Version 1.1 TU Delft Open, Delft, p. 577. http://dx.doi.org/10.5074/T.2021.001, URL: https://textbooks.open.tudelft.nl/textbooks/catalog/book/37.

Deltares, 2018. Delft3D-Flow User Manual. Technical Report, p. 712.

Eliot, M.J., Travers, A., Eliot, I., 2006. Morphology of a low-energy beach, como beach, western Australia. J. Coast. Res. 221, 63–77. http://dx.doi.org/10.2112/05A-0006.1, URL: http://www.bioone.org/doi/abs/10.2112/05A-0006.1.

Jackson, N.L., Nordstrom, K.F., Eliot, I., Masselink, G., 2002. 'Low energy' sandy beaches in marine and estuarine environments: a review. Geomorphology 48 (1–3), 147–162. http://dx.doi.org/10.1016/S0169-555X(02)00179-4.

Liu, S., Ye, Q., Wu, S., Stive, M.J., 2018. Horizontal circulation patterns in a large shallow lake: Taihu lake, China. Water (Switzerland) 10 (6), http://dx.doi.org/10.3390/w10060792.

Lorang, M.S., Stanford, J.A., Hauer, F.R., Jourdonnais, J.H., 1993. Dissipative and reflective beaches in a large lake and the physical effects of lake level regulation. Ocean Coast. Manag. 19 (3), 263–287. http://dx.doi.org/10.1016/0964-5691(93)90045-Z.

Nordstrom, K.F., Jackson, N.L., 2012. Physical processes and landforms on beaches in short fetch environments in estuaries, small lakes and reservoirs: A review. Earth-Sci. Rev. 111 (1–2), 232–247. http://dx.doi.org/10.1016/j.earscirev.2011.12.004.

Nutz, A., Schuster, M., Ghienne, J.F., Roquin, C., Bouchette, F., 2018. Wind-driven waterbodies: a new category of lake within an alternative sedimentologically-based lake classification. J. Paleolimnol. 59 (2), 189–199. http://dx.doi.org/10.1007/s10933-016-9894-2.

Rijkswaterstaat, 2018. Peilbesluit IJsselmeergebied. Technical Report, URL: https://www.helpdeskwater.nl/@185393/peilbesluiten/.

Rijkswaterstaat, 2019. Houtribdijk reinforcement. URL: https://www.rijkswaterstaat.nl/en/about-us/gems-of-rijkswaterstaat/houtribdijk-reinforcement.

Schuster, M., Roquin, C., Duringer, P., Brunet, M., Caugy, M., Fontugne, M., Mackaye, H.T., Vignaud, P., Ghienne, J.F., 2005. Holocene lake mega-chad palaeoshorelines from space. Quat. Sci. Rev. 24 (16–17), 1821–1827. http://dx.doi.org/10.1016/j.quascirev.2005.02.001.

Ton, A.M., Vuik, V., Aarninkhof, S.G., 2021. Sandy beaches in low-energy, non-tidal environments: Linking morphological development to hydrodynamic forcing. Geomorphology 374, 107522. http://dx.doi.org/10.1016/j.geomorph.2020.107522.

Van Kessel, T., Gerben, D.B., Boderie, P., 2008. Calibration Suspended Sediment Model Markermeer. Technical Report, Deltares.

Van Ledden, M.R.H., Gerrits, G.R.H., Van Kessel, T.W.D.H., Mosselman, E.W.D.H., 2006. Verdiepingsslag en Maatregelen Slibproblematiek Markermeer: Analyse Kennisleemten En Inventarisatie Maatregelen. Technical Report.

Van Leeuwen, C.H., Temmink, R.J., Jin, H., Kahlert, Y., Robroek, B.J., Berg, M.P., Lamers, L.P., Van den Akker, M., Posthoorn, R., Boosten, A., Olff, H., Bakker, E.S., 2021. Enhancing ecological integrity while preserving ecosystem services: Constructing soft-sediment islands in a shallow lake. Ecol. Solut. Evid. 2 (3), 1–10. http://dx.doi.org/10.1002/2688-8319.12098.

Vijverberg, T., 2008. Mud Dynamics in the Markermeer. Silt Traps as a Mitigation Measure for Turbidity (MSc. thesis). p. 162.

Vila-Concejo, A., Gallop, S.L., Largier, J.L., 2020. Sandy beaches in estuaries and bays. In: Jackson, D., Short, A.D. (Eds.), Sandy Beach Morphodynamics. Elsevier Ltd, pp. 343–362. http://dx.doi.org/10.1016/B978-0-08-102927-5/00015-1, Chapter 15.